Ursolic acid loaded-mesoporous hydroxylapatite/ chitosan therapeutic scaffolds promote the bone regeneration

Xijiao Yu (yayiyu@163.com)
Shanghai 9th Peoples Hospital Affiliated to Shanghai Jiaotong University School of Medicine
Yuxuan Wang
Shanghai 9th Peoples Hospital Affiliated to Shanghai Jiaotong University School of Medicine
Xiao-Liang Liu
Shanghai 9th Peoples Hospital Affiliated to Shanghai Jiaotong University School of Medicine
Degang Yu
Shanghai Jiao Tong University School of Medicine
Shanyong Zhang
Shanghai 9th Peoples Hospital Affiliated to Shanghai Jiaotong University School of Medicine

Research

Keywords: Mesoporous Hydroxylapatite, Bone Regeneration, Ursolic acid, Drug Delivery

Posted Date: October 1st, 2020

DOI: https://doi.org/10.21203/rs.3.rs-84118/v1

Abstract

Background: Mesoporous hydroxylapatite (MHAP) could play an important role in bone regeneration, and UA (Ursolic acid) also promote the osteogenic differentiation. Accordingly, we developed the UA loaded MHAP scaffolds to cure bone defects. In vitro, we synthesize biomaterial scaffolds. By SEM, XRD, EDS and FTIR, we test the performance of the hybrid scaffolds. By drug release, ALP staining, Alizarin red staining, and Western blotting, we test the osteo-inductive properties of scaffold materials. In vivo, We verify bone regeneration through a rat skull defect model.

Results: The MHAP is a rod-shaped structure with a length of 100~300nm and a diameter of 40~60nm. The critical structure gives the micro scaffold a property of control release due to the pore sizes of 1.6~4.3 nm in hydroxyapatite and the hydrogen bonding between the scaffolds and UA drugs. The released UA drugs could notably promote the expression of osteogenic-related genes (COL1, ALP, OPG) and osteogenic-related proteins (BMP-2, RUNX2 and COL1). Both the images of μCT and the results of double fluorochrome labelling demonstrated that therapeutic scaffolds promoted the bone regeneration. We obtained the similar results through immunohistochemistry.

Conclusions: The MHAP-CS-UA scaffolds have good osteo-inductivity and bone regeneration. And they will be the novel and promising candidates to cure the bone disease.

1. Background

Craniomaxillofacial (CMF) bone damage, surgical, infection and bone disease can result in serious bone defects [1–4]. All of those bone defects brought the high burden to patients both on economic and spiritual [5, 6]. Traumatic surgeons and scientists find many ways to solve these problems like xenografts, allografts and autograft [7–9]. Good postoperative outcomes achieved by these surgery methods. However, we cannot ignore the deficiency of them, for example donor-site morbidity for autografts; immunogenicity for xenografts and allografts [10, 11]. Consequently, the new way to rescue the bone defects is urgent to find.

The other way to maintain this medical demand is to develop the new bone repair materials which should exhibit osteo-inductivity, biocompatibility and osteo-conductivity [12–15]. Mesoporous hydroxylapatite was given great hope to play a proper role on bone repair due to its biocompatibility and osteo-conductivity [16, 17]. After implantation of hydroxyapatite scaffolds in vivo, the carbonated hydroxyapatite layer can be formed between the scaffolds and the host bone, but its osteogenic ability is not enough to effectively repair bone defects, especially for patients with bone diseases [18]. However, as a drug delivery system, the layered porous structure and mesoporous properties of hydroxyapatite scaffolds provide a large surface area for bone deposition and drug delivery. In addition, as an important natural biomaterial, chitosan (cs) has good biocompatibility and antimicrobial activity [19]. Its functional groups such as ~ OH and ~ NH2 in CS could up-regulate drug release behavior through hydrogen bond interaction [20–22].

Ursolic acid (UA) is a traditional medicinal plant in China. It has many biological characteristics, including anti-cancer, anti-inflammatory, anti-virus, anti-bacterial, anti-diabetes, cardiovascular, anti-bacterial and anti-oxidative activities [23–26]. At present, most studies on ursolic acid (UA) focus on signal transduction pathways, such as transforming growth factor beta (TGF-β)/SMAD signal transduction, mitogen-activated protein kinase (MAPK) and nuclear factor κB (NF-κB) [27, 28]. Other studies have shown that ursolic acid can increase the expression of osteoblast-specific protein by activating BMP-2/Smad4 signaling pathway or Wnt/β-catenin signaling pathway [29]. In addition, as far as we know, ursolic acid (UA) is seldom used for bone regeneration [29]. Therefore, the application of UA in hydroxyapatite scaffolds is an ideal and attractive method for related diseases.

In vitro, the physiological abilities of MHAP-CS-UA were evaluated by CCK, ALP, Alizarin red, RT-PCR and western blot (WB). In vivo, a critical size skull defect was established to assess the difference in the ability of MHAP-CS-UA and MHAP-CS scaffolds to accelerate bone repair. In this study, MHAP-CS scaffolds loaded with UA (MHAP-CS-UA) were prepared. The steps are as follows: (i) MHAP microspheres were prepared by hydrothermal method using CTAB as organic template; (i) MHAP-CS porous scaffolds were synthesized by freeze-drying method; and (i i) UA drugs were loaded into the scaffolds. Interestingly, we found that MHAP-CS-UA scaffolds had good biocompatibility, and the drug released from the treatment scaffolds significantly enhanced the expression of osteogenesis-related genes and accelerated the regeneration of new bone in vivo.

2. Material And Methods

2.1. Synthesis of MHAP scaffolds

All of the chemical reagents were purchased from sigma. The synthetic process of the MHAP scaffolds is as follows. Weighing 0.251 CTAB (mCTAB/(theoretical output mCa5(PO4)3.OH)*100 = 5%) and adding 100 ml deionized water, stirring for 10 minutes, dissolving completely, and then putting into 90℃ oil bath. Next, weighing 4.0018 g (0.03 mol) (NH4) 2HPO4 and dissolving in CTAB solution, stirring for 20 minutes, 280r/min to make 0.05M solution. After 20 minutes, adjusting the pH value of solution with ammonia water is 10.5. And then 11.9268 g (0.05 mol) Ca (NO3) 2.4H2O was dissolved in pure water to prepare 100 ml, 0.3M solution. The pH value of the solution was adjusted by ammonia water to be 10.5. The solution in previous step was slowly dripped into the solution of step 2 for about 40 minutes. The whole process keeps the solution PH = 10.5 unchanged, stirring for 2 hours, 280 r/min, and aging at 90 ℃ for 12 hours. Then, Wash with deionized water to neutral then with ethanol for 1–2 times. Next, drying at 80 ℃ for 24 hours; grinding. Finally, Calcination, 2 degree/minute heating, 900 degree heat preservation for 4 hours, natural cooling to room temperature, grinding.

2.2. Synthesis of MHAP-CS hybrid scaffolds

Preparation of Chitosan (CS) Solution: 2 g Chitosan is dissolved in 50 ml 2 vol% acetic acid solution (1:25), stirred mechanically for 3 hours until completely dissolved, 320r/min. Next, weighing 2 g mesoporous hydroxyapatite powder (MHAP) and slowly adding it into CS solution, stirring and dispersing

for 2 h (mass ratio: MHAP: CS = 1:1). Then, transfer the dispersed and uniform solution to 24 mesh cell culture medium, transfer it to the magnetic field of − 20 C refrigerator for 24 hours, and then transfer it to freeze-dryer for freeze-drying after freezing: cooling to − 56 C (taking about 4 hours), freeze-drying with vacuum less than 10 Pa (about 96 hours in winter and 72 hours in summer); the formed samples were immersed in 10 wt% NaOH solution for 1 day, washed repeatedly to PH = 7 (to wash for 5 days, change water three times a day), and then freeze-dried again (about 1 day). Finally, the preparation of mesoporous hydroxyapatite/chitosan composite scaffolds can be obtained by cutting brittle fracture in liquid nitrogen.

2.3. Drug loading-release tests of MHAP-CS-UA hybrid scaffolds

First, ursolic acid powder was formulated into a solvent of 1 mg/ml. Next, 2.2835 mL of the above ursolic acid solution was taken up and placed in a 50 mL volumetric flask. And then anhydrous ethanol was added to the volumetric flask to prepare a 100 umol ursolic acid solution. The prepared ursolic acid scaffold material(1 μM) is used for sustained drug release. The scaffold material (5 μM, 10 μM) operates as described above.

The release test of the MHAP-CS-UA (1 μM, 5 μM, 10 μM) drug scaffold material was carried out after immersing in 5.0 ml of phosphate buffer solution (PBS), and the above operations were carried out under normal temperature and an oscillation atmosphere of 80 rpm. We extracted 1.0 ml of the above solution at different time points (3, 6, 9, 12, 24, 48 and 72 h) while adding an equal volume of PBS solution. Finally, the corresponding drug concentration was analyzed by high performance liquid chromatography (HPLC, Agilent 1100, US).

2.4. Material characterization

The morphologies of MHAP microspheres and MHAP-CS composite scaffolds were studied by scanning electron microscopy (SEM) and characterized by energy dispersive spectroscopy (EDS). The study used transmission electron microscopy to detective nano-mesoporous structures of MHAP microspheres. Also analyzed the porous structure of MHAP by automatic surface area and porosity analyzer at 80K. The pore size distribution of MHAP was calculated by Barrett-Joyner-Halenda (BJH) method. The phase compositions of MHAP-CS and MHAP-CS-UA composite scaffolds were analyzed by X-ray powder diffraction (XRD; D/Max III C, Japan). At last, Fourier transform infrared spectroscopy identified the functional groups in MHAP-CS and MHAP-CS-UA composite scaffolds.

2.5. Cell viability and attachment

MC3T3-E1 cells were purchased from Shanghai Institute of Biological Sciences, Chinese Academy of Sciences. Human bone marrow mesenchymal stem cells from Shanghai Rochen Biotechnology Co., Ltd. (Shanghai, China). The cells were cultured in 10% fetal bovine serum and 1% penicillin/streptomycin medium at 37 °C, and 1×10^4 MC3T3-E1 cells were seeded into 96 well plated. After 24 hours, the medium was replaced with MHAP-CS or MHAP-CS-UA scaffold extract. The cell counting kit 8 was cultured for

1 day, 2 days, and 3 days, respectively. hBMSC was used as a cell model to detect the adhesion of cells on different scaffolds. Each scaffold was inoculated with 1×10^4 h BMCs into 24-well plates. hBMSCs were cultured for 12 hours and washed with phosphate. Buffered saline (PBS) was then fixed with 2.5% glutaraldehyde for 20 minutes. The HBMSCs were washed 3 times with phosphate buffered saline (PBS). The samples were dehydrated with ethanol at a concentration gradient of 75, 85, 95 and 100. Finally, the morphology of hBMSCs was characterized by scanning electron microscopy (SEM; FEI; Thermo Fisher Scientific, Inc.) on the scaffold with a magnification of 10 kV.

2.6. In vitro tests of osteogenic capability

The detection of differentiation of hBMSCs is based on alkaline phosphorylation (ALP, Renbao, Shanghai, China) and alizarin red staining (AR, Sigma-Aldrich). 1×10^4 hBMSCs were inoculated into 24-well plants for 24 hours and cultured with MHAP-CS, MHAP-CS-UA scaffolds. After 7 and 14 days of culture, hBMSCs were immobilized with 4% paraformaldehyde. Wash hBMSC 3 times with phosphate buffer saline (PBS). Next, stained hBMSC with ALP kit and alizarin red kit. Next, the residual substance of the above reagent is washed away with PBS. Finally, the samples stained with the above alkaline phosphatase and alizarin red were photographed by an inverted phase contrast microscope.

The expression levels of osteogenesis-related genes, including alkaline phosphorylation (ALP), collagen 1 (COL1) and osteoprotegerin (OPG) were detected by real-time quantitative polymerase chain reaction RT-PCR. 4×10^6 MC3T3-E1 cells were seeded in a 6-well plate containing the extract of the above scaffold material. Seven days later, total RNA was collected by RNeasy Mini kit (Qiagen, Inc., Valencia, CA, USA) and reverse transcribed into cDNA (Takara Bio, Inc., Otsu, Japan). The SYBR Premix Ex Taq kit (Takara Biotechnology Co., Ltd.) and an ABI 7500 Sequencing Detection System (Applied Biosystems; Thermo Fisher Scientific, Inc.) was used to perform qPCR. Glyceraldehyde-3-phosphate dehydrogenase (GAPDH) gene expression was used as a standard reference, the following thermocycling conditions were used: 40 cycles of denaturation at 95˚C for 5 s and amplification at 60˚C for 24 s. And the data were calculated by $2^{\Delta\Delta Ct}$ method. All the above steps are in accordance with the instructions of the reagent manufacturer. The PCR primers were designed as follows:

GAPDH forward 5'-CACCACCATGGAGAAGGCCG-3'

and reverse 5'-ATGATGTTCTGGGCAGCCCC-3'

OPG forward 5'-CGAGCGCAGATGGATCCTAA-3'

And reverse 5'-CCACATCCAACCATGAGCCT-3'

Col1 forward 5'- GCTCCTCTTAGGGGCCACT-3'

And reverse 5'- CCACGTCTCACCATTGGGG-3'

ALP forward 5'- CATCATCATGTTCCTGGGAG-3'

And reverse 5'- GACCTGAGCGTTGGTGTTGT-3'

MC3T3-E1 cells were cultured in the medium of MHAP/CS or MHAP-CS-UA scaffolds to measure the expression of osteoblast-related proteins (BMP-2, COL1, RUNX2, Smad1/5). Protein was extracted from the radioimmunoprecipitation assay (RIPA) lysis buffer (cat. no. C500005; Sangon Biotech Co., Ltd.) containing 1 μM protease inhibitor. Then centrifuge at a speed of 12,000 rpm for 10 minutes. The bicinchoninic acid assay (BCA) method was used to detect the corresponding protein concentration. Gel electrophoresis was carried out on SDS-PAGE and transferred to PVDF membrane. Close the film with 5% milk for 1 hour. The membrane and the first antibody were incubated overnight at 4 degrees. After 24 hours, the membrane was washed with PBS three times and incubated with the second antibody coupled with horseradish peroxidase for 1 hour. Finally, the horseradish peroxidase-conjugated secondary antibodies reactivity was detected by the Odyssey infrared imaging system (LI-COR Biosciences, Lincoln, NE, USA).

2.7. In vivo tests of osteogenic capability

The Animal Research Committee of the Ninth People's Hospital Affiliated to the Medical College of Shanghai Jiao Tong University approved all the animal experiments in this experiment. Fifteen Sprague-Dawley female rats (200–250 g) were selected. A bilateral critical size skull defect model was used to evaluate bone regeneration. The diameter and height of bone defect were 5 mm and 2 mm respectively. MHAP-CS and MHAP-CS-UA stents (n = 5) were filled in the defect area and the scalp was sutured. Multicolor continuous fluorescence labeling was used to characterize the formation and mineralization of new bone. Alizarin red (30 mg/kg, Sigma-Aldrich) and calcein (30 mg/kg, Sigma-Aldrich) were injected intraperitoneally to label the animals 3 and 21 days before euthanasia. Twelve weeks later, the animals were euthanized. The bilateral critical size skull defects were isolated from the surrounding tissues. Samples were immersed in formalin solution buffered by 4% phosphate for 7 days, and then detected by micro-CT system (Skyscan 1072; Skyscan, Aartselaar, Belgium). The parameters are set to 90KV voltage, 88uA current and 28um voxel size. After the scanning is completed, the 3D image is reconstructed. Bone healing was evaluated by calculating bone mineral density (BMD) and new bone mass/tissue volume (BV/TV). Undecalcified samples were embedded in polymethyl methacrylate. The sagittal section of the skull was cut 150 mm thick with a slicer (Leica, Hamburg, Germany). Multicolor continuous fluorescence labeling (Leica, Heidel-berg, Germany; alizarin red: 543/580–670 nm, calcein: 488/500–550 nm) was observed under confocal laser scanning microscopy. The mineralization rate is quantified by brightness analysis system based on different color bands. Soft tissue around the skull was removed and immersed in 10% EDTA for 30 days. And then embedded in paraffin. Histological sections were prepared for Masson staining and immunohistochemistry of BMP-2, COL-1, RUNX2 and OPG protein. Finally, they were observed in a light microscopy (magnification, x10). Images were analyzed using Image-Pro Plus 6.0(Media Cybernetics, Inc., Rockville, MD, USA).

2.8. Statistical analysis

All the data were expressed as means ± standard deviation (SD) and were analyzed using one-way ANOVA. *P < 0.05 was considered statistically significant.

3. Results And Discussion

3.1. Morphologies and structures of MHAP nanoparticles

As shown in Fig. 1a, b, MHAP was a short rod-like structure with a length of 100–300 nm and a diameter of 40–60 nm. Figure 1c showed the N2 adsorption desorption isotherms of the MHAP nanoparticles. The type III isotherms with type H3 hysteresis loops further demonstrated the presence of mesopores within the MHAP nanoparticles. The mesopore sizes were mainly distributed at approximately 2.2 ~ 23.3 nm, as revealed by the DFT pore size distribution curve (Fig. 1d). The mesoporous structure of MHAP nanoparticles provided good basic conditions for material degradation and drug loading. MHAP had great application potential as an engineering material for bone tissue repair, but its osteo-inductivity needed to be improved, so as to better meet the clinical needs [30–32]. Considering that MHAP had the ability to load drugs, we chose to load UA into it. The UA drug was extracted from many plants such as the whole grass of the Labiatae plant, Prunella vulgaris, and the leaves of the holly, holly, iron holly leaves [33]. The UA is a triterpenoid compound found in natural plants and has many biological effects such as sedative [34], anti-inflammatory [35], antibacterial [36], and immune defense responses [37]. The Ursolic acid (UA), also promote osteoblast differentiation and new bone formation.

3.2. Morphology and structures of MHAP-CS hybrid scaffolds

If the usual mode of administration, such as oral or intravenous, is used, the biological activity of the drug may be difficult to achieve maximum efficiency. Here, we first created the MHAP-CS-UA composite scaffold as the drug delivery system for UA. The MHAP-CS scaffold was prepared by freeze-drying technology using MHAP nanoparticles and CS as raw materials. Interestingly, the MHAP-CS scaffold exhibited a three-dimensional interconnected macroporous structure with pore sizes of approximately 100 ~ 300 μm (Fig. 2a). The surface of the scaffolds was inlaid with many rod-like structures to obtain MHAP powder, which were evenly distributed (Fig. 2b, c). The Ca, and P elements were originated from the MHAP nanoparticles, the C element was originated from the CS and the O element was originated from both the MHAP and CS. The C element distribution images in Fig. 2d, the Ca element distribution images in Fig. 2e, the O element distribution images in Fig. 2f, and the P element distribution images in Fig. 2g. Figure 2h was an electron microscope scan image of the surface of the MHAP-CS scaffold. Figure 2i was the merge image of the above elements. The EDS of the MHAP/CS hybrid scaffolds indicated that the main chemical elements included C, Ca, O and P (Fig. 2j). Figure 2k, l indicated XRD patterns and the FTIR spectra of MHAP nanoparticles, CS powders, MHAP-CS and MHAP-CS-UA hybrid scaffolds. MHAP-CS and MHAP-CS-UA contained MHAP diffraction peaks. CS was a semi-crystalline material, and its diffraction peak was located at 2θ = 28.01°. Moreover, the functional groups of the samples were characterized by FTIR spectra. The OH group located at around 3440 cm^{-1}. For the CS powders, MHAP-CS and MHAP-CS-

UA scaffold, the band at around 2920 cm^{-1} corresponded to the ~ CH2 and ~ CH stretching vibration. The band at 1550 cm^{-1} was assigned to N–H bending vibration. The bands due to the bending vibration of phosphate (PO43-) groups located at 566 and 602 cm^{-1}, and the bands due to the stretching vibration located at 1093 and 1031 cm^{-1}. The band at 1384 cm^{-1} was the interference peak of the instrument.

3.3. Drug release property of MHAP-CS-UA therapeutic scaffolds

The MHAP-CS scaffold has outstanding performance as a carrier, which is mainly related to its special structure. The MHAP-CS composite scaffold has interconnected macroporous structure with pore sizes of approximately 100 ~ 300 μm, which were originated from the sublimation of frozen solvent during the freeze-drying process (Fig. 2a). These mesoporous structures are the locations where the drug is loaded. In addition, within the MHAP nanoparticles, N2 adsorption desorption isotherms proved the existence of mesopores in MHAP nanoparticles. The mesopore size is mainly distributed in about 2.2 ~ 23.3 nm. The mesoporous structure of MHAP nanoparticles provided good basic conditions for material degradation and drug loading (Fig. 1). MHAP nanoparticles are widely and evenly distributed in the scaffold material (Fig. 2b, c). In addition, many of the polar functional groups present in the MHAP-CS composite scaffold can adsorb drug molecules on the surface of the scaffold by hydrogen bonding, thereby achieving controlled drug release (Fig. 2k, i). Therefore, we design different concentrations of scaffold materials for drug release experiments. Different concentrations of UA and MHAP-CS were made into composite scaffolds with different drug concentrations. In the drug release test, MHAP-CS-UA (1 μM), MHAP-CS-UA (5 μM) and MHAP-CS-UA (10Mm) were immersed in PBS, and the corresponding drug concentrations were determined by high performance liquid chromatography. Characterization. All samples showed similar drug release trends (Fig. 3a). The UA drug is rapidly released from the drug carrier within 24 hours, and the release rate begins to decrease over time. After 72 hours, the UA drug concentrations released from MHAP-CS-UA (1 μM), MHAP-CS-UA (5 μM), and MHAP-CS-UA (10 μM) reached 0.033 μM, 0.171 μM, and 0.342 μM, respectively (Fig. 3b-d).

3.4. In vitro cytocompatibility and osteo-inductivity of MHAP-CS-UA therapeutic scaffolds

We applied proliferation and cell adhesion assays to detect the biocompatibility of MHAP-CS-UA scaffolds. The proliferation ability of the cells was examined by co-culture with MC3T3-E1 cells using different concentrations of samples. The results obtained by the CCK-8 method (Fig. 4a) showed that the all groups were active. This result demonstrates that the UA released by the MHAP-CS-UA treatment scaffold is less toxic to MC3T3-E1 cells. However, they could promote the proliferation of MC3T3-E1 cells. By scanning electron microscopy, we found that hBMSC was evenly distributed on the MHAP-CS and MHAP-CS-UA scaffold (Fig. 4d), indicating that the MHAP-CS-UA scaffold has excellent cell compatibility.

It is well known that the protein essential for early bone formation is alkaline phosphatase, which is a major component of extracellular matrix mineralization, and calcium nodule, which also represents the ability of bone mineralization. Figure 4b, c show ALP staining and Alizarin red staining images of hBMSCs after 7 days and 21 days of treatment in the blank control group, MHAP-CS and MHAP-CS-UA groups. The order of the osteogenesis and bone mineralization ability shown in these three groups was: the largest in the MHAP-CS-UA group, the second in the MHAP-CS group, and finally the blank group.

The expression levels of the ALP, RUNX2 and COL1 proteins were analyzed using MHAP-CS group and the blank scaffold as a control group to evaluate the osteo-inductive effect of the MHAP-CS-UA scaffold (Fig. 4e). The results showed that the expression of osteogenic related proteins was up-regulated compared to the control group. In addition, the MHAP-CS-UA group also expressed higher levels of expression of and P-Smad1/5 than the control group. Similar results were obtained at the gene level (Fig. 4f, i, j), and the expression levels of ALP, COL1 and OPG in the MHAP-CS-UA group was up-regulated compared to the control and the MHAP-CS group.

3.5. In vivo bone regeneration property of MHAP-CS-UA therapeutic scaffolds

The MHAP-CS-UA scaffold was evaluated for bone regeneration by establishing a rat skull defect model (Fig. 5). Three-dimensional reconstruction of CT images showed that after 12 weeks of establishment of the rat skull defect model, no new bone formation was observed in the blank control group and some new bone formation was evident in the MHAP-CS and MHAP-CS-UA groups (Fig. 5a). Quantitative results show that MHAP-CS-UA has an increase in volume and density of new bone formation compared to MHAP-CS (Fig. 5b). In addition, different bone mineral density(BMD) values were detected in the three groups in the following order: MHAP-CS-UA group > MHAP-CS group > blank group (Fig. 5c).

Histomorphometry of new bone formation and mineralization with alizarin red and calcein fluorescence showed that the average distance between the MHAP-CS and MHAP-CS-UA groups were greater than that of the control group (Fig. 6a, b). The above conclusions confirmed that the mineralization rate of the MHAP-CS-UA group(6.12 ± 0.21 μm/day) was higher than that of the vehicle group(4.24 ± 0.25 μm/day) and the blank group(2.11 ± 0.16 μm/day). In addition, Masson staining showed that the blank group showed a large amount of fibrous tissue and a small amount of newly formed bone around the defect site, while the MHAP-CS-UA and MHAP-CS scaffold were more collagen and new bone formation (Fig. 6c). Compared with the MHAP-CS group, the new group had more new bone, suggesting that the released UA can promote the mineralization of the osteogenic tissue.

Osteoblast-associated protein expression in scaffold materials was detected by immunohistochemistry. We performed immunohistochemistry using tissue sections from each of the control group, MHAP-CS group and MHAP-CS-UA group (Fig. 7). The oteogenic related proteins (OPG, RUNX-2, COL1, BMP-2) were detected. We found that the expression of MHAP-CS-UA proteins (OPG, RUNX-2, COL1, BMP-2) were significantly higher than that of the MHAP-CS group. In addition, protein expression in the MHAP-CS

group was also significantly enhanced compared to the control group. This further showed that MHAP-CS-UA would promote bone repair by releasing UA.

4. Conclusion

In summary, the ideas for making MHAP-CS-UA treatment scaffolds are as follows: (i) synthesis of mesoporous MHAP scaffold; (ii) preparation of drug carrier MHAP-CS; (iii) formation of MHAP-CS-UA after UA loading Treatment of the scaffold. Porosity of 100 ~ 300 μm promotes the regeneration of collagen and the differentiation of new bone tissue. The hydrogen bonding between the mesoporous structure and the polar group in the scaffold enhances the controlled release capacity of UA. The drug UA in the vector significantly enhanced the expression of genes and proteins related to new bone formation and differentiation. The animal experimental rat skull defect model further proved the above viewpoint. Therefore, the MHAP-CS-UA scaffold has good performance. It will play an important role in osteogenic differentiation and new bone regeneration.

Declarations

Acknowledgements

We thank the laboratory members for reagents and assistance with

experiments.

Ethics approval and consent to participate

The present study was supported by the department of Orthopedic Surgery, Shanghai Ninth People's Hospital, Shanghai Jiao Tong University School of Medicine.

Authors' contributions

XY and YW conceived the rationale and designed the research;XL performed the experiments, analyzed data and wrote the paper; DY performed the experiments; SZ revised the manuscript. All authors read and approved the final manuscript.

Consent for publication

All authors agree to publish this manuscript

Availability of data and material

The data that support the findings of this study are available from the corresponding author upon reasonable request.

Competing interests

The authors declare no competing financial interest.

Abbreviations

chitosan (CS), Ursolic acid (UA), Mesoporous hydroxylapatite(MHAP), scanning electron microscopy (SEM, energy-dispersive spectrometry (EDS), X-ray diffractometer (XRD), Fourier transform infrared spectroscopy (FTIR), X-ray photoelectron spectroscopy (XPS), bone marrow mesenchymal stem cells (hBMSCs), α-minimum essential medium (α-MEM), foetal bovine serum (FBS), Cell Counting Kit-8 (CCK-8), phosphate-buffered saline (PBS), alkaline phosphatase (ALP), paraformaldehyde (PFA), horseradish peroxide (HRP), Institutional Animal Care and Use Committee (IACUC), bone mineralization density (BMD), new bone volume/tissue volume (BV/TV), 10% ethylene diamine tetraacetic acid (EDTA).

References

1. Aghaloo TL, Chaichanasakul T, Bezouglaia O, Kang B, Franco R, Dry SM. E. AttiS. Tetradis. Osteogenic potential of mandibular vs. long-bone marrow stromal cells. J Dent Res. 2010;89:1293–8.
2. Bai X, Lu S, Liu H, Cao Z, Ning P, Wang Z, Gao C, Ni B. D. MaM. Liu. Polysaccharides based injectable hydrogel compositing bio-glass for cranial bone repair. Carbohydr Polym. 2017;175:557–64.
3. Sumathra M, Sadasivuni KK. S. S. KumarM. Rajan. Cisplatin-Loaded Graphene Oxide/Chitosan/Hydroxyapatite Composite as a Promising Tool for Osteosarcoma-Affected Bone Regeneration. ACS Omega. 2018;3:14620–33.
4. Tao J, Zhang Y, Shen A, Yang Y, Diao L, Wang L, CaiY D. Hu. Injectable Chitosan-Based Thermosensitive Hydrogel/Nanoparticle-Loaded System for Local Delivery of Vancomycin in the Treatment of Osteomyelitis. Int J Nanomedicine. 2020;15:5855–71.
5. Toledano M, Toledano-Osorio M, Osorio R, Carrasco-Carmona A, Gutierrez-Perez JL, Gutierrez-Corrales A, Serrera-Figallo MA, LynchD CD. Torres-Lagares. Doxycycline and Zinc Loaded Silica-Nanofibrous Polymers as Biomaterials for Bone Regeneration. Polymers (Basel). 2020; 12.
6. Liu L, Jin R, Duan J, Yang L, Cai Z, Zhu W, Nie Y, He J, Xia C, Gong Q, Song B. J. M. AndersonH. Ai. Bioactive iron oxide nanoparticles suppress osteoclastogenesis and ovariectomy-induced bone loss through regulating the TRAF6-p62-CYLD signaling complex. Acta Biomater. 2020;103:281–92.
7. Lavanya K, Chandran SV, BalagangadharanN K. Selvamurugan. Temperature- and pH-responsive chitosan-based injectable hydrogels for bone tissue engineering. Mater Sci Eng C Mater Biol Appl. 2020;111:110862.
8. Gashtasbi F, Hasannia S, Hasannia S, Mahdi Dehghan M, SarkaratA F. Shali. Comparative study of impact of animal source on physical, structural, and biological properties of bone xenograft. Xenotransplantation. 2020; e12628.
9. Chen Y, Li W, Zhang C, WuJ Z. Liu. Recent Developments of Biomaterials for Additive Manufacturing of Bone Scaffolds. Adv Healthc Mater. 2020; e2000724.

10. Gronbach L, Wolff C, Klinghammer K, Stellmacher J, Jurmeister P, Alexiev U, Schafer-Korting M, Tinhofer I. U. KeilholzC. Zoschke. A multilayered epithelial mucosa model of head neck squamous cell carcinoma for analysis of tumor-microenvironment interactions and drug development. Biomaterials. 2020;258:120277.
11. He F, Springer NL, Whitman MA, Pathi SP, Lee Y, Mohanan S, Marcott S, Chiou AE, Blank BS, Iyengar N, Morris PG, Jochelson M, Hudis CA, Shah P, Kunitake J, Estroff LA. J. LammerdingC. Fischbach. Hydroxyapatite mineral enhances malignant potential in a tissue-engineered model of ductal carcinoma in situ (DCIS). Biomaterials. 2019;224:119489.
12. Zhang M, Shi J, Xie M, Wen J, Niibe K, Zhang X, Luo J, Yan R, Zhang Z. H. EgusaX. Jiang. Recapitulation of cartilage/bone formation using iPSCs via biomimetic 3D rotary culture approach for developmental engineering. Biomaterials. 2020;260:120334.
13. Li Y, Jahr H. J. ZhouA. A. Zadpoor. Additively manufactured biodegradable porous metals. Acta Biomater. 2020.
14. Lu Y, Li L, Lin Z, Wang L, Lin L, Li M, Zhang Y, Yin Q. Q. LiH. Xia. A New Treatment Modality for Rheumatoid Arthritis: Combined Photothermal and Photodynamic Therapy Using Cu7.2 S4 Nanoparticles. Adv Healthc Mater. 2018;7:e1800013.
15. Liu DD, Zhang JC, Zhang Q, WangM SX. Yang S. TGF-beta/BMP signaling pathway is involved in cerium-promoted osteogenic differentiation of mesenchymal stem cells. J Cell Biochem. 2013;114:1105–14.
16. Wang HNieCH. Fabrication and characterization of PLGA/HAp composite scaffolds for delivery of BMP-2 plasmid DNA. J Control Release. 2007;120:111–21.
17. Hou LT, Tsai AY. C. M. LiuF. Feng. Autologous transplantation of gingival fibroblast-like cells and a hydroxylapatite complex graft in the treatment of periodontal osseous defects: cell cultivation and long-term report of cases. Cell Transplant. 2003;12:787–97.
18. Henkel KO, Gerber T, Dorfling P, Hartel J, Jonas L. K. K. GundlachV. Bienengraber. [Stimulating regeneration of bone defects by implantation of bioceramics and autologous osteoblast transplantation]. Mund Kiefer Gesichtschir. 2002;6:59–65.
19. Radwan NH, Nasr M, Ishak RAH, AbdeltawabG NF. A. S. Awad. Chitosan-calcium phosphate composite scaffolds for control of post-operative osteomyelitis: Fabrication, characterization, and in vitro-in vivo evaluation. Carbohydr Polym. 2020;244:116482.
20. Sadeghianmaryan A, Naghieh S, Sardroud HA, Yazdanpanah Z, Soltani YA. J. SernagliaX. Chen. Extrusion-based printing of chitosan scaffolds and their in vitro characterization for cartilage tissue engineering. Int J Biol Macromol. 2020.
21. Ansari Z, Kalantar M, Soriente A, Fasolino I, Kharaziha M. L. AmbrosioM. G. Raucci. In-Situ Synthesis and Characterization of Chitosan/Hydroxyapatite Nanocomposite Coatings to Improve the Bioactive Properties of Ti6Al4V Substrates. Materials (Basel). 2020; 13.
22. Lastra ML, Gomez RibellesA JL. Cortizo M. Design and characterization of microspheres for a 3D mesenchymal stem cell culture. Colloids Surf B Biointerfaces. 2020;196:111322.

23. Porwal K, Pal S, Dev K, China SP, Kumar Y, Singh C, Barbhuyan T, Sinha N, Sanyal S, Trivedi AK. R. MauryaN. Chattopadhyay. Guava fruit extract and its triterpene constituents have osteoanabolic effect: Stimulation of osteoblast differentiation by activation of mitochondrial respiration via the Wnt/beta-catenin signaling. J Nutr Biochem. 2017;44:22–34.
24. Li Q, Fan YS, Gao ZQ. K. FanZ. J. Liu. Effect of Fructus Ligustri Lucidi on osteoblastic like cell-line MC3T3-E1. J Ethnopharmacol. 2015;170:88–95.
25. Lee SU, Park SJ, Kwak HB, Oh J. Y. K. MinS. H. Kim. Anabolic activity of ursolic acid in bone: Stimulating osteoblast differentiation in vitro and inducing new bone formation in vivo. Pharmacol Res. 2008;58:290–6.
26. Tan H, Zhao C, Zhu Q, Katakura Y, Tanaka H. K. OhnukiK. Shimizu. Ursolic Acid Isolated from the Leaves of Loquat (Eriobotrya japonica) Inhibited Osteoclast Differentiation through Targeting Exportin 5. J Agric Food Chem. 2019;67:3333–40.
27. Jiang C, Xiao F, Gu X, Zhai Z, Liu X, Wang W, Tang T, Wang Y, Zhu Z, Dai K, QinJ A. Wang. Inhibitory effects of ursolic acid on osteoclastogenesis and titanium particle-induced osteolysis are mediated primarily via suppression of NF-kappaB signaling. Biochimie. 2015;111:107–18.
28. Peng M, Qiang L, Xu Y, Li C, LiJ T. Wang. Modification of Cysteine 179 in IKKbeta by Ursolic Acid Inhibits Titanium-Wear-Particle-Induced Inflammation, Osteoclastogenesis, and Hydroxylapatite Resorption. Mol Pharm. 2018;15:5244–51.
29. Ge YW, Lu JW, Sun ZY, Liu ZQ, Zhou J, Ke QF, Mao YQ. Y. P. GuoZ. A. Zhu. Ursolic acid loaded-mesoporous bioglass/chitosan porous scaffolds as drug delivery system for bone regeneration. Nanomedicine. 2019;18:336–46.
30. Szewczyk A, Skwira A, Konopacka A, Sadej R, WalkerM G. Prokopowicz. Mesoporous silica pellets as bifunctional bone drug delivery system for cefazolin. Int J Pharm. 2020;588:119718.
31. Li C, Qin W, Lakshmanan S, Ma X, SunB X. Xu. Hydroxyapatite based biocomposite scaffold: A highly biocompatible material for bone regeneration. Saudi J Biol Sci. 2020;27:2143–8.
32. Carvalho Vasconcelos R, Ferreira C, de Araujo EM, Motta F, Bomio M, de Araujo Junior RF, Paiva DFF, Pirih FQ, da Silva JSP, Chan AB, Cruz LJ, Ishii M, de Medeiros C. G. Coelho Bernardo GuerraA. A. de Araujo. Zirconia/hydroxyapatite (80/20) scaffold repair in critical size calvarial defect increased FGF-2, osteocalcin and OPG immunostaining and IL-10 levels. Am J Transl Res. 2020;12:2439–50.
33. Pitaloka DAE, Cooper AM, Artarini AA, DamayantiE S. Sukandar Y. Regulation of mitogen-activated protein kinase signaling pathway and proinflammatory cytokines by ursolic acid in murine macrophages infected with Mycobacterium avium. Infect Dis Rep. 2020;12:8717.
34. Deciga-Campos M, Cortes A, Pellicer F, Diaz-RevalM I. Gonzalez-Trujano E. Isobolographic analysis of the antinociceptive interaction between ursolic acid and diclofenac or tramadol in mice. Planta Med. 2014;80:139–45.
35. Wang C, Gao Y, Zhang Z, Chen C, Chi Q, XuL K. Yang. Ursolic acid protects chondrocytes, exhibits anti-inflammatory properties via regulation of the NF-kappaB/NLRP3 inflammasome pathway and ameliorates osteoarthritis. Biomed Pharmacother. 2020;130:110568.

36. Qian W, Li X, Shen L, Wang T, Liu M, Zhang J, Yang M. X. LiC. Cai. Antibacterial and antibiofilm activity of ursolic acid against carbapenem-resistant Enterobacter cloacae. J Biosci Bioeng. 2020;129:528–34.
37. Ahn YJ, Wang L, FosterR S. Asmis. Dietary 23-Hydroxy Ursolic Acid Protects Against Diet-Induced Weight Gain and Hyperglycemia by Protecting Monocytes and Macrophages Against Nutrient Stress-Triggered Reprogramming and Dysfunction and Preventing Adipose Tissue Inflammation. J Nutr Biochem. 2020; 108483.

Figures

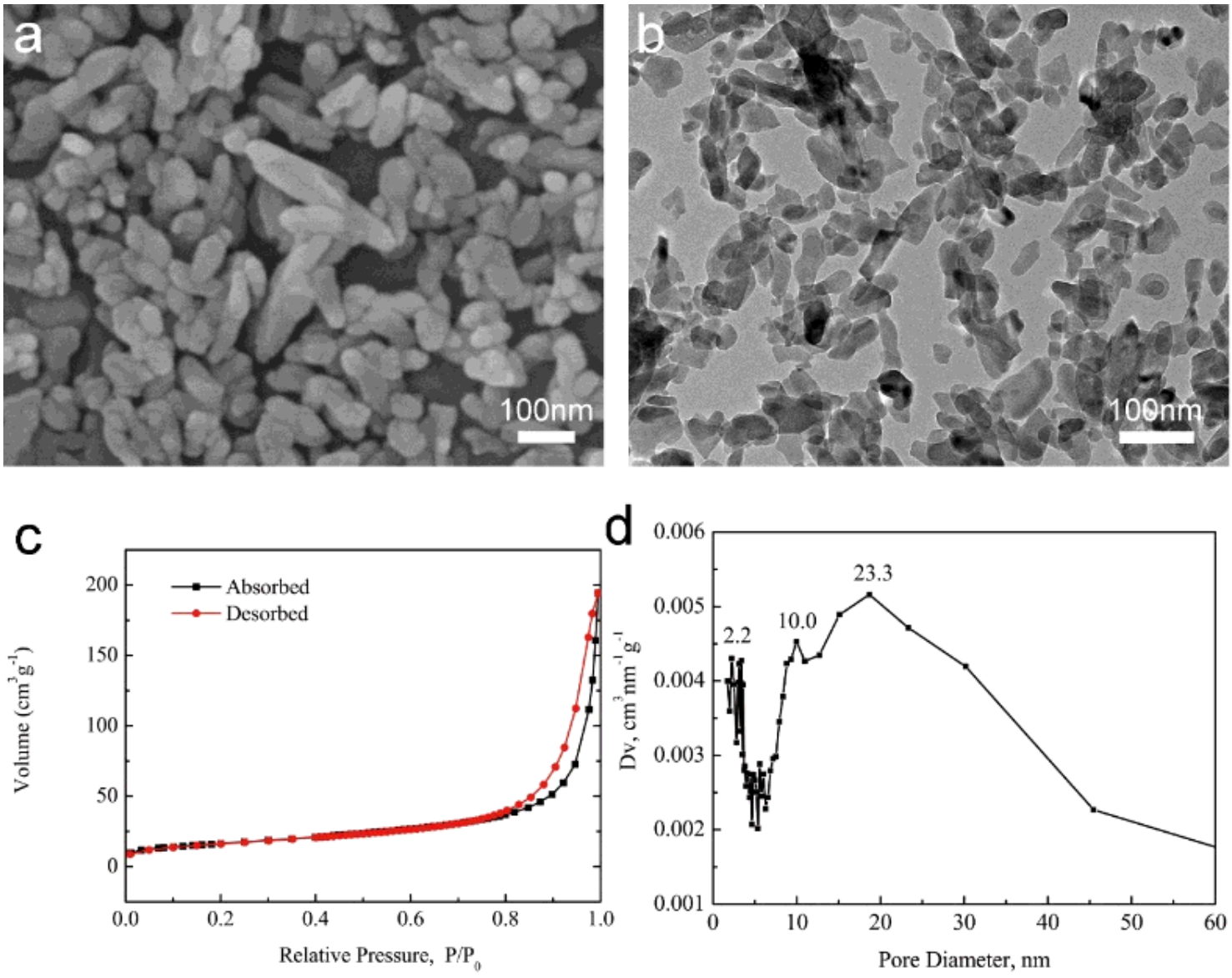

Figure 1

Characterization of MHAP nanoparticles: (a) SEM image; (b) TEM image; (c) N2 adsorption–desorption isotherms; and (d) BJH pore size distribution curve.

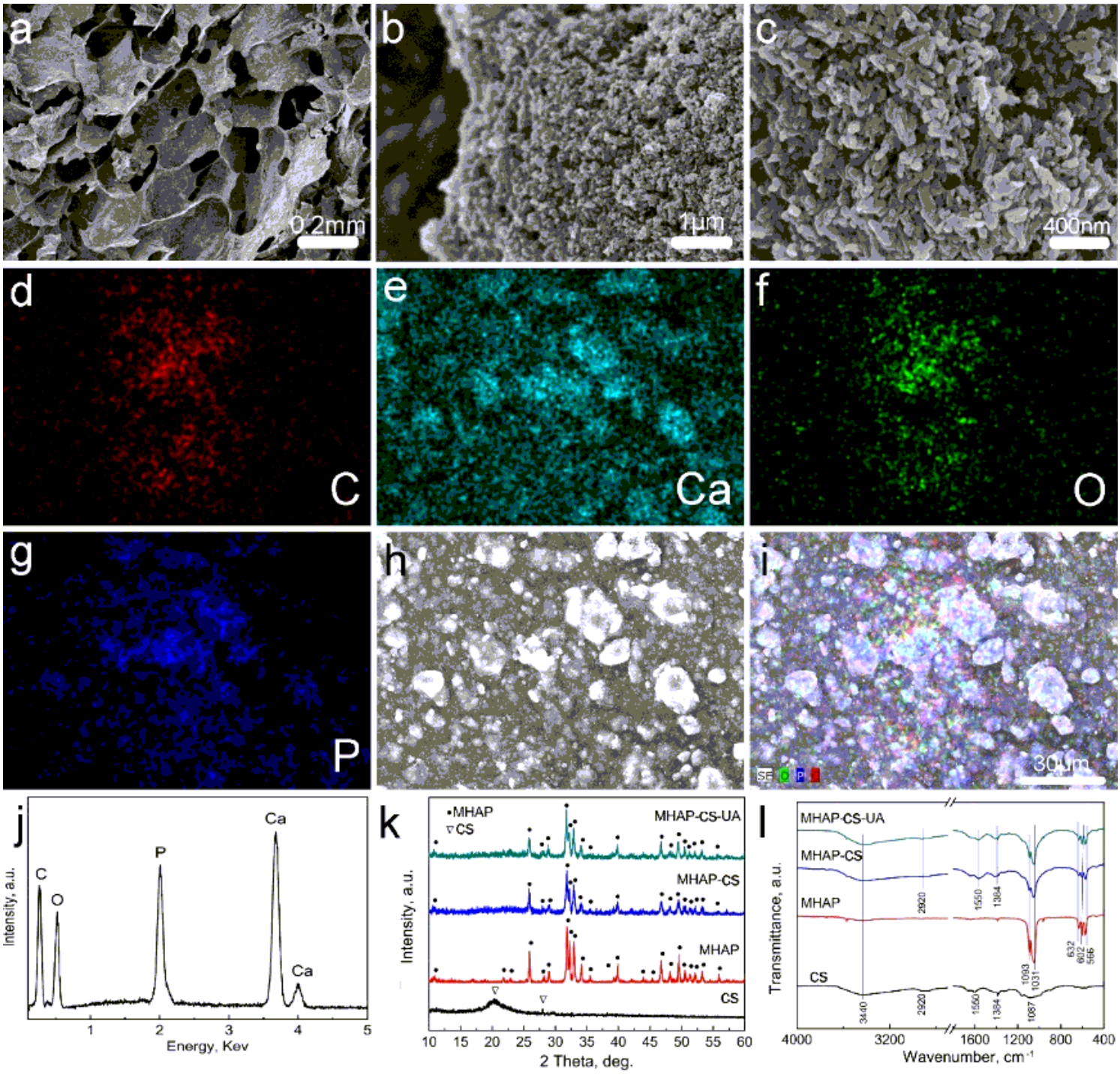

Figure 2

(a) Low-resolution SEM image; (b, c) high-resolution SEM image; (d~i) C, Ca, O and Pelement distribution image; (j) EDS pattern; (k) XRD patterns and (l) FTIR spectra of MHAP nanoparticles, CS powders, MHAP-CS and MHAP-CS-UA hybrid scaffolds.

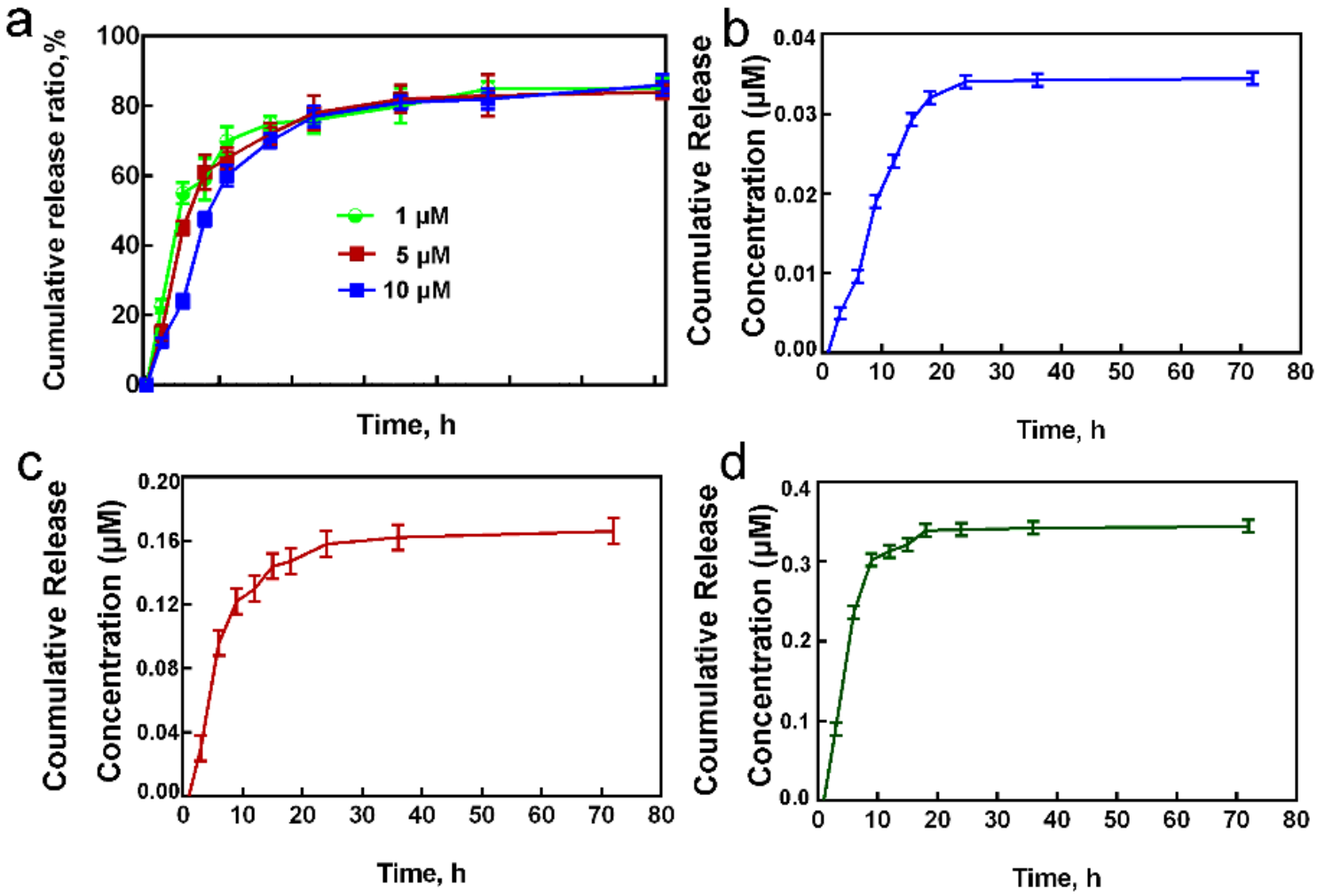

Figure 3

The release of drugs at different concentrations. (a) The cumulative drug release ratios for different MHAP-CS-UA scaffolds. MHAP-CS-UA (1μM), (B) MHAP-CS-UA (5μM) and (C) MHAP-CS-UA (10μM).

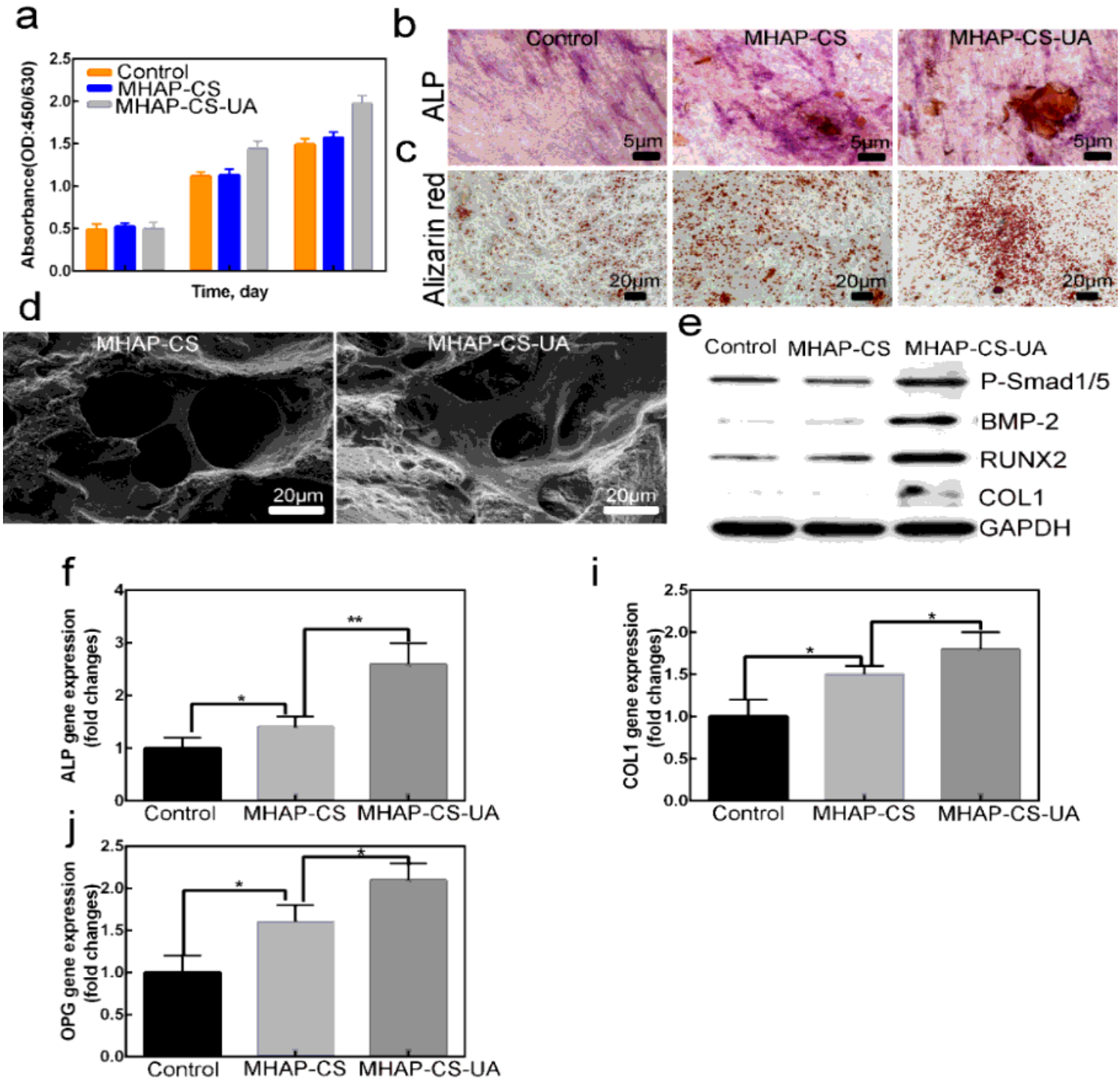

Figure 4

In vitro experiments on scaffolds. (a) CCK-8; (b, c) ALP staining and Alizarin red staining; (d) Scanning electron microscope (SEM) of scaffolds; (e) Detect protein expression level by Western blot; (f, i, j) Detect gene expression level by PCR.

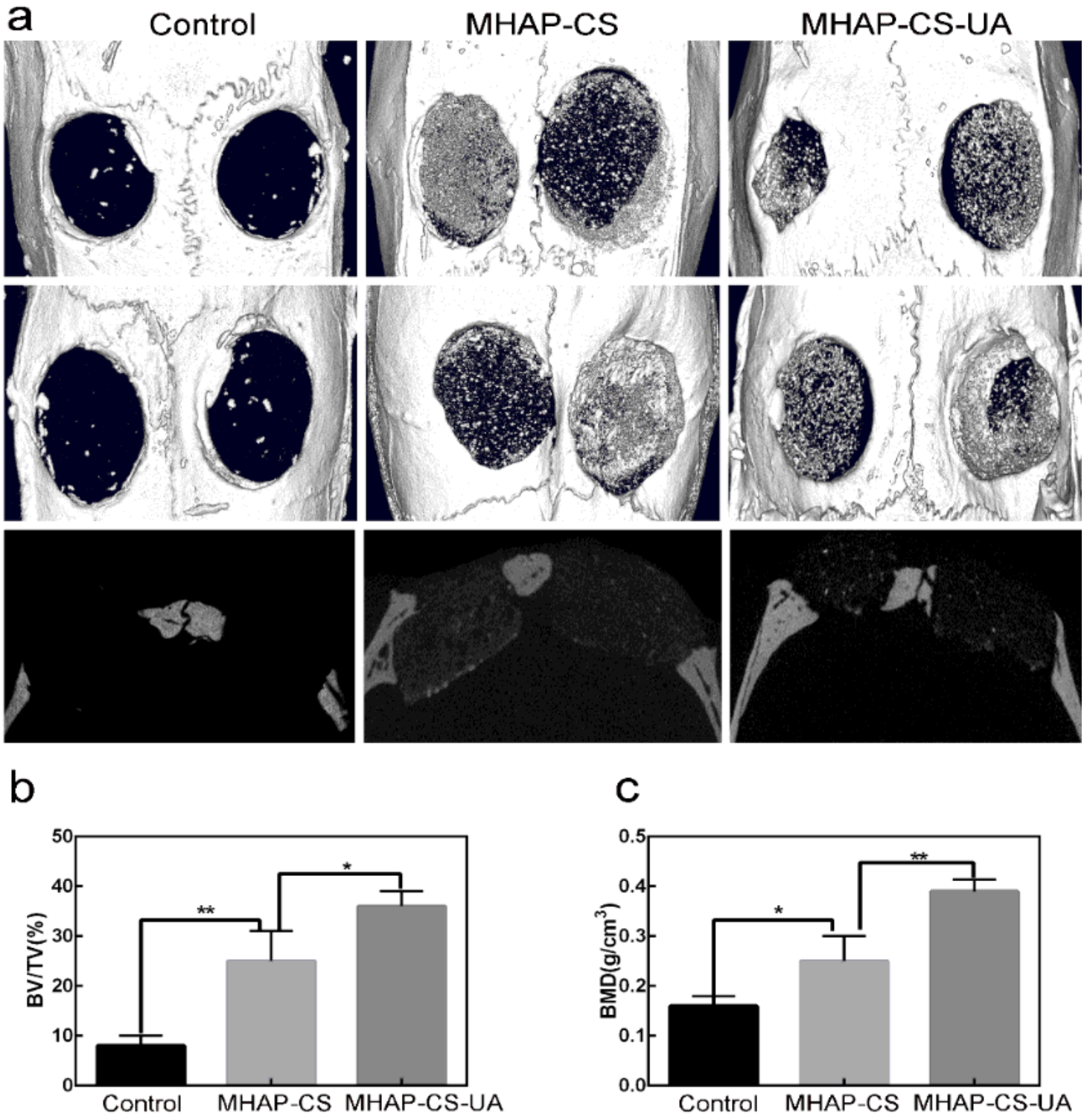

Figure 5

In vivo osteogenic activity of scaffolds. (a) Micro-CT images of calvarial defects model; (b) New-bone volume/tissue volume (BV/TV); (c) morphometric analysis of bone mineral density (BMD).

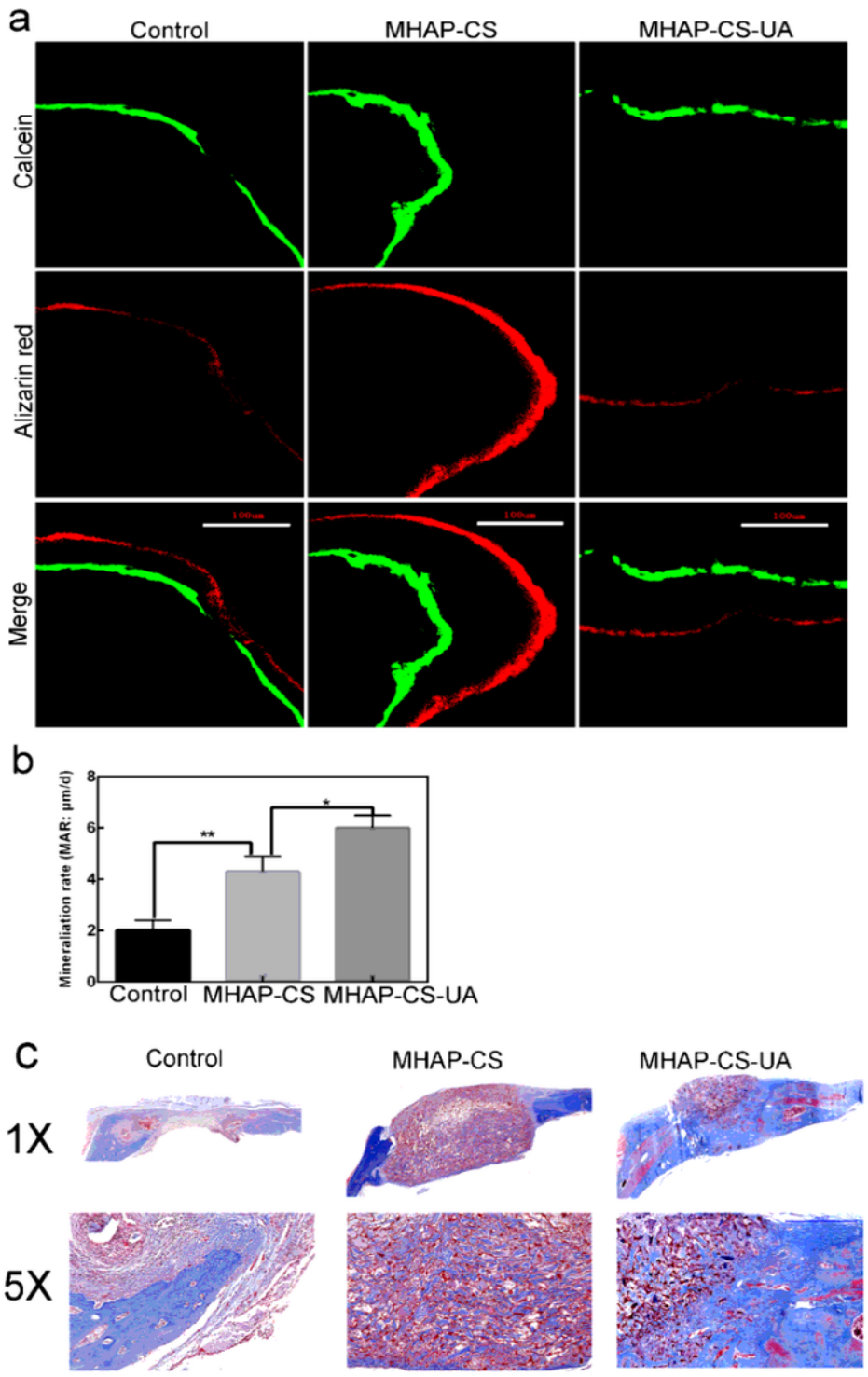

Figure 6

(a) The green and red lines represent the 3 weeks and 3 days before euthanasia, respectively. The last line is the merged images; (b) Mineralization rate (the average distance between two lines divided by the number of days); (c) By Masson's trichrome staining, histomorphological analysis for determining newly formed bones (blue) and collagen components (red).

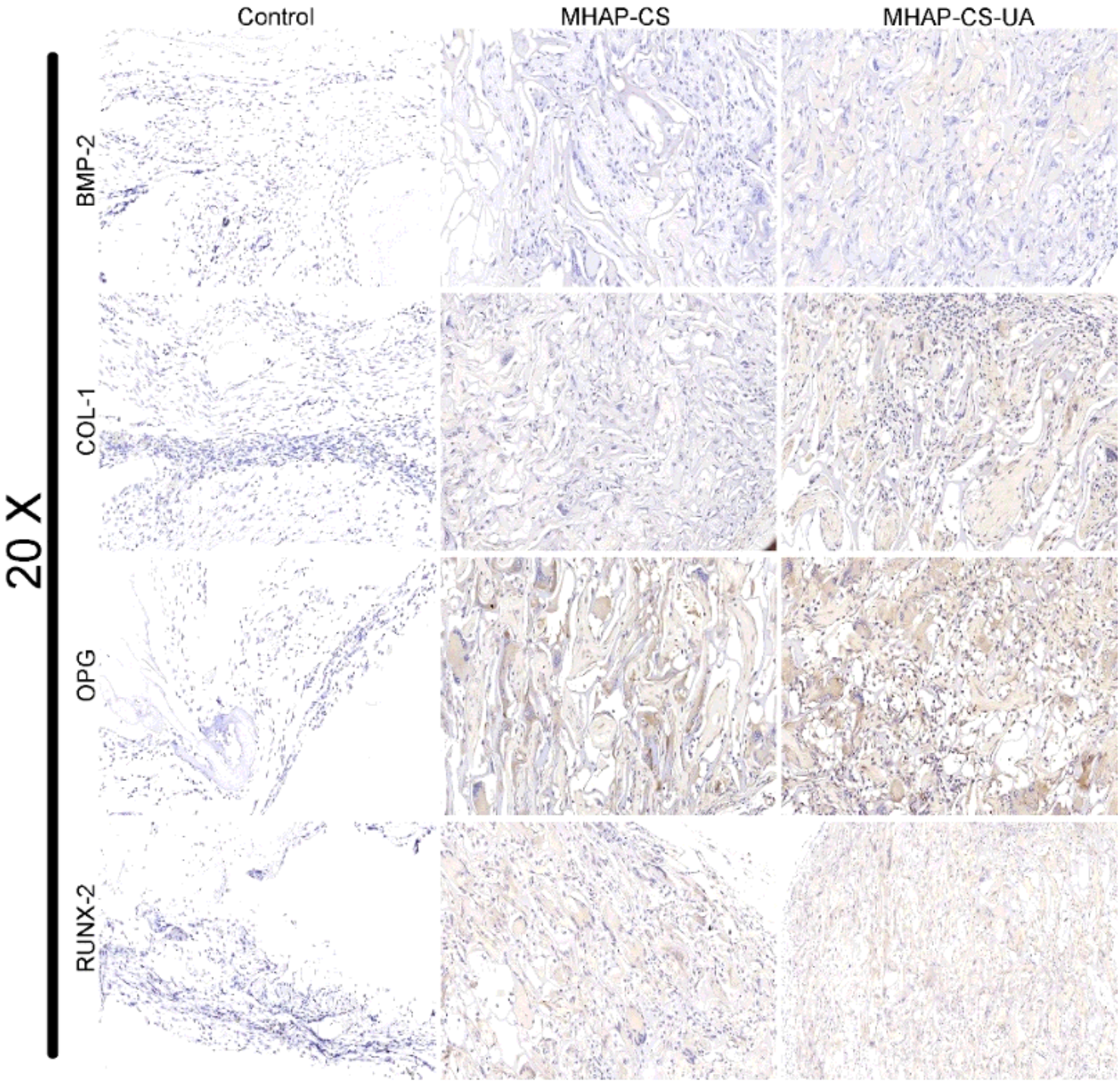

Figure 7

By immunohistochemistry, observed BMP-2, COL 1, OPG and RUNX-2 in the control group, MHAP-CS group and MHAP-CS-UA group.